SIAM J. SCI. COMPUT.
Vol. 42, No. 3, pp. B656–B674

A SPECTRAL ALGORITHM FOR THE TIME-DEPENDENT KOHN–SHAM EQUATIONS: ACCURATELY TREATING EXTERNAL POTENTIALS BASED ON FROZEN GAUSSIAN APPROXIMATIONS*

RICARDO DELGADILLO† AND DI LIU†

Abstract. In this paper, we develop a novel spectral method for solving the time-dependent Kohn–Sham equations in the semiclassical regime. Our strategy is to use a single-step predictor-corrector algorithm, where the propagator is derived using a Fourier integral operator commonly known as the frozen Gaussian approximation (FGA) ansatz. In the case of laser potentials, we derived a simplified FGA to avoid the high dimensional integration. Numerical examples are provided to verify applicability, as well as efficiency and accuracy of the scheme.

Key words. time dependent density functional theory, frozen Gaussian approximation, spectral method, scientific computing, quantum chemisty

AMS subject classifications. 49M, 65C, 65Z

DOI. 10.1137/19M1245104

1. Introduction.

We are interested in developing an efficient numerical algorithm for the time-dependent density functional theory (TDDFT) by approximating solutions to the time-dependent Kohn–Sham (TDKS) equations:

$$\mathrm{i}\hbar\partial_t\phi_j(\boldsymbol{r},t) = -\frac{\hbar^2}{2m}\nabla^2\phi_j(\boldsymbol{r},t) + \frac{e^2}{4\pi\epsilon_0}v_s[\rho](\boldsymbol{r},t)\phi_j(\boldsymbol{r},t) \quad \text{for} \quad j=1,\dots,N, \tag{1.1}$$

where $\mathrm{i}=\sqrt{-1}$, $\hbar$ is the reduced Planck constant, m and e are the mass and charge of an electron, and ϵ_0 is the permittivity of free space. The complex valued Kohn–Sham orbitals $\{\phi_j(\boldsymbol{r},t)\}_{j=1}^N$ have the corresponding occupation numbers $\{f_j\}_{j=1}^N$, and the time-dependent electron density is given by

$$\rho(\boldsymbol{r},t) = \sum_{j=1}^{N} f_j|\phi_j(\boldsymbol{r},t)|^2. \tag{1.2}$$

Integer N is the number of valence electrons for the system of interest. $v_s[\rho]$ is the noninteracting Kohn–Sham potential:

$$v_s[\rho](\boldsymbol{r},t) = v_0(\boldsymbol{r},t) + v_h[\rho](\boldsymbol{r},t) + v_{xc}[\rho](\boldsymbol{r},t) + v_{ext}(\boldsymbol{r},t). \tag{1.3}$$

For simplicity, we will also assume that the nuclear coordinates are fixed. The first term on the right-hand side of (1.3) is the nuclear potential, which we will approximate using pseudopotentials. The Hartree potential v_h is given by

$$v_h[\rho](\boldsymbol{r},t) = \int \frac{\rho(\boldsymbol{r}',t)}{|\boldsymbol{r}-\boldsymbol{r}'|}d\boldsymbol{r}'. \tag{1.4}$$

*Submitted to the journal's Computational Methods in Science and Engineering section February 15, 2019; accepted for publication (in revised form) January 6, 2020; published electronically May 14, 2020.

https://doi.org/10.1137/19M1245104

Funding: This work was supported by NSF through grants NSF DMS 1720002 and DMS 1418959.

†Department of Mathematics, Michigan State University, East Lansing, MI 48824 (delgadi3@msu.edu, liudi1@msu.edu).

$v_h(\boldsymbol{r})$ is also the solution of the Poisson equation:

$$\nabla^2 v_h(\boldsymbol{r}) = -4\pi\rho(\boldsymbol{r}), \tag{1.5}$$

and is usually more efficiently computed by solving (1.5). The third term $v_{xc}(\boldsymbol{r}, t)$ is the exchange-correlation potential, for which we will choose the adiabatic local density approximation (ALDA) satisfying the following form:

$$v_{xc}[\rho](\boldsymbol{r}, t) = -C_X \rho^{1/3}(\boldsymbol{r}, t), \tag{1.6}$$

with $C_X = (\frac{3}{\pi})^{1/3}$. Notice that the ALDA is just the local density approximation (LDA) of ground state density functional theory (DFT) with $\rho(\boldsymbol{r})$ replaced with $\rho(\boldsymbol{r}, t)$ [15, 21]. We also note that the adiabatic approximation is a good approximation for systems whose density is varying slowly with time. The final term in v_s is the time-dependent external potential. We will assume our system initially to be in the ground state which will be computed using the ground state Kohn–Sham equations. Our discussion will be focused on 3-dimensional systems.

Due to the nonlinearity of the TDKS equations, we are planning to solve it self-consistently. Therefore, a crucial step for arriving at an algorithm for solving the TDKS equations is to numerically obtain a solution to the linear Schrödinger equation:

$$\mathrm{i}\hbar\partial_t\phi = -\frac{\hbar^2}{2m}\nabla^2\phi + V(\boldsymbol{r}, t)\phi, \qquad \phi_0(\boldsymbol{r}) \in L^2(\mathbb{R}^3). \tag{1.7}$$

Specifically, for the full TDKS equations, the linearized equation (1.7) will be solved for each of the N orbitals on the time interval $[t_i, t_{i+1}]$ with $V(\boldsymbol{r}, t)$ set to be the Kohn–Sham potential (1.3) evaluated with initial values at $t = t_i$ for $i = 1, 2, \ldots, M$. One of the earliest approximations for solving (1.7) includes the WKB method, which adopts the following ansatz:

$$\phi_{WKB}(\boldsymbol{r}, t) = A(\boldsymbol{r}, t)e^{\mathrm{i}S(\boldsymbol{r},t)/\hbar},$$

where A and S are expanded as $A = A_0 + A_1\hbar + A_2\hbar^2 + \cdots$ and $S = S_0 + S_1\hbar + S_2\hbar^2 + \cdots$. The first order terms, A_0 and S_0, satisfy

$$\partial_t\rho + \nabla_{\boldsymbol{r}} \cdot (\rho\nabla S_0) = 0, \qquad A_0(\boldsymbol{r}, 0) = A_{in}(\boldsymbol{r}),$$

with $\rho(\boldsymbol{r}, t) = |A_0(\boldsymbol{r}, t)|^2$, and

$$\partial_t S_0 + \frac{1}{2}|\nabla S_0|^2 + V(\boldsymbol{r}, t) = 0, \qquad S_0(\boldsymbol{r}, 0) = S_{in}(\boldsymbol{r}), \tag{1.8}$$

i.e., $\rho(\boldsymbol{r}, t)$ is described by a transport equation, and S_0 satisfies an Eikonal equation. These equations are independent of $\hbar$ and therefore can be efficiently solved numerically.

However, the major drawback of the WKB ansatz is the breakdown of the solution where the Hamilton–Jacobi equation (1.8) develops singularities [6, 19, 20]. For this reason, the Gaussian beam (GB) method [22, 11] was introduced by Popov to overcome the problem of undefined solutions at caustics. The difference between the GB method and the WKB method is that the GB method uses a complex phase function such that

$$T(t, \boldsymbol{r}, \boldsymbol{r}') = S(t, \boldsymbol{r}') + \boldsymbol{p}(\boldsymbol{r}', t) \cdot (\boldsymbol{r} - \boldsymbol{r}') + \frac{1}{2}(\boldsymbol{r} - \boldsymbol{r}')^T M(\boldsymbol{r}', t)(\boldsymbol{r} - \boldsymbol{r}') + \mathcal{O}(|\boldsymbol{r} - \boldsymbol{r}'|^3)$$

with $S \in \mathbb{R}$, $\boldsymbol{p} \in \mathbb{R}^3$, and $M \in \mathbb{C}^{3\times 3}$. The imaginary part of $M(\boldsymbol{r}', t)$ is chosen to be positive definite and one can show that it remains like this for $t > 0$. Therefore, the solution retains a Gaussian profile and decays exponentially as the distance between $\boldsymbol{r}$ and the center of the Gaussian $\boldsymbol{r}'$ increases. The solution to the linear Schrödinger equation is then constructed by summation of the beams:

$$\phi_{GB}(\boldsymbol{r}, t) = \left(\frac{1}{2\pi\hbar}\right)^{\frac{3}{2}} \int_{\mathbb{R}^3} A(t, \boldsymbol{r}') e^{\mathrm{i}T(t,\boldsymbol{r},\boldsymbol{r}')/\hbar}\, d\boldsymbol{r}'.$$

Clearly T is a Taylor expansion about $\boldsymbol{r}'$, and as a result there is a growing error for large $\boldsymbol{r} - \boldsymbol{r}'$. This is the main difficulty with the GB method and is known as *splitting of the beams*.

The problem with the splitting of the beams has been overcome by using Gaussian functions of fixed width, which is known as the frozen Gaussian approximation (FGA). The idea of using nonspreading wave packets for quantum dynamics has been proposed by Herman and Kluk in [10]. The propagator in [10] is known as the Herman–Kluk propagator which our FGA method is based on. Rigorous mathematical justification of the Herman–Kluk propagator can be found in [25]. We note that the FGA can also be applied to many other equations; see [12, 13, 14] for examples different from the Schrödinger equation. In this paper, we will be using the first order FGA solution for the linear Schrödinger equation:

(1.9)
$$\phi_{\mathrm{FGA}}(\boldsymbol{r}, t) = \frac{1}{(2\pi\hbar)^{9/2}} \int_{\mathbb{R}^9} A(t, \boldsymbol{q}, \boldsymbol{p}) G_{\boldsymbol{q},\boldsymbol{p}}(\boldsymbol{r}) e^{\mathrm{i}S(t,\boldsymbol{q},\boldsymbol{p})/\hbar} \overline{G}_{\boldsymbol{q},\boldsymbol{p}}(\boldsymbol{r}') \phi_0(\boldsymbol{r}')\, d\boldsymbol{r}'\, d\boldsymbol{q}\, d\boldsymbol{p},$$

where $G_{\boldsymbol{q},\boldsymbol{p}}(\boldsymbol{r})$ are Gaussian functions depending on phase space coordinates $(\boldsymbol{q}, \boldsymbol{p})$:

$$G_{\boldsymbol{q},\boldsymbol{p}}(\boldsymbol{r}) = \exp\left(-\frac{1}{2\hbar}|\boldsymbol{r} - \boldsymbol{q}|^2 + \mathrm{i}\frac{\boldsymbol{p}}{\hbar} \cdot (\boldsymbol{r} - \boldsymbol{q})\right).$$

To avoid numerically dealing with the above high dimensional integration, we will derive simplified formulas for (1.9) so it can be reduced to a 3-dimensional integral, under the assumption that the external potential is of the following form commonly used in lasers:

$$V(\boldsymbol{r}, t) = \boldsymbol{\alpha} \cdot \boldsymbol{r} f(t), \tag{1.10}$$

where $\boldsymbol{\alpha}$ is a polarization vector. The resulting integral operator can then be computed quickly using the fast Fourier transform, which will enable us to design a solver faster than standard finite difference or finite element methods. Another major advantage of using the FGA integral operator is that it treats the external potential for lasers exactly. This will lead to a more rapid self-consistent convergence when compared to other spectral methods, such as the Strang-splitting spectral method [5], which require a numerical approximation for $V_{ext}(\boldsymbol{r}, t)$.

A similar approach has been proposed based on the implicit midpoint discretization such that

$$\mathcal{U}_{CN}(t + \Delta t, t) := \frac{1 - \frac{\mathrm{i}}{2}\Delta t \widehat{H}(t + \Delta t/2)}{1 + \frac{\mathrm{i}}{2}\Delta t \widehat{H}(t + \Delta t/2)},$$

which will lead to the Crank–Nicolson method, and also must be solved self-consistently. Generalizations include the exponential midpoint and the enforced time-reversal symmetry method, and a summary can be found in [7]. The main difference between these

methods and our scheme is that we use a splitting technique along with the spectral method to solve the linear Schrödinger equation, instead of inverting a Hamiltonian matrix. Another difference is that we treat the external potential in the Hamiltonian exactly, instead of using a midpoint approximation.

In this paper, we will formulate the FGA method by providing a solution to the semiclassical Schrödinger equation that depends on a parameter ε, which is obtained by rescaling the space and time of the system. As a result, the value of $\hbar$ will be replaced by that of ε, which will facilitate the FGA ansatz. The situation of $\varepsilon = 1$ will recover the classical system with atomic units. The main advantage for our algorithm is its efficiency in the semiclassical regime $0 < \varepsilon \ll 1$, which corresponds to the situation in the limit as the number of particles in the system approaches infinity. Depending on the features of the potential, the Crank–Nicolson scheme needs step sizes $o(\varepsilon)$ in time and space [16], which is also true if one uses the Dufort–Frankel method [17]. One can improve this to $\Delta x = \mathcal{O}(\varepsilon)$ and $\Delta t = o(\varepsilon)$ by using the time-splitting spectral method [5]. Now compare this with (1.9); one only needs to require Δx to be on the order of the width of the Gaussian functions or, equivalently, $\Delta x = \mathcal{O}(\sqrt{\varepsilon})$. For the time scale, as shown later, the ODEs governing $(\boldsymbol{q}, \boldsymbol{p}, S, a)$ do not depend on ε and take only a $\Delta t = \mathcal{O}(1)$ computational load. One more benefit of using the FGA ansatz is that by approximating the solution of a PDE through an ODE, it is much more efficient to use in high dimensions compared with nonasymptotic methods.

Semiclassical methods have been used to study physical phenomena such as the Bose–Einstein condensate (see [4]). In this situation ε is typically a number much less than 1. When the pseudopotential is periodic, the semiclassical Schrödinger equation has also been used to model semiconductor materials (see [23] for a review of a variety of models for semiconductor device simulation). However, in this paper we will be focusing the application of our algorithm on simulating finite systems such as metal clusters.

The rest of the paper is organized as follows: in section 2, we will give a short summary of TDDFT and the Kohn–Sham equations. Background on the FGA method can be found in section 3. In section 4, we will introduce our FGA-based algorithm for the TDKS equations. Section 5 will provide several numerical examples. We make some concluding remarks and discuss future works in section 6.

2. Time-dependent density functional theory. In this section, we will briefly review the main aspects of the TDDFT and fix some notations. For more background on this topic, see [9, 26, 18].

2.1. Time-dependent many-body Schrödinger equation. The goal of TDDFT is to obtain observable information on the electronic and molecular structures by solving the time-dependent electron density. This is done by simplifying the time-dependent many-body Schrödinger equation which, in the Born–Oppenheimer approximation, is given by

$$\mathrm{i}\hbar\partial_t\psi = \left(\widehat{T} + \widehat{V}(t) + \widehat{W}\right)\psi. \tag{2.1}$$

The kinetic energy operator is defined as

$$\widehat{T} = \sum_{j=1}^{N} -\frac{\hbar^2}{2m}\nabla_j^2,$$

and the electron-electron interaction potential is of the form

$$\widehat{W} = \frac{e^2}{4\pi\epsilon_0} \sum_{j \neq k}^{N} \frac{1}{|\boldsymbol{r}_j - \boldsymbol{r}_k|},$$

where e is the unit of charge, and N is the number of electrons in the system. Here $\psi(\boldsymbol{r}_1, \ldots, \boldsymbol{r}_N, t)$ is a complex valued wave function depending on the electronic coordinates $\boldsymbol{r}_j$ for each $j \in 1, \ldots, N$. In general, not only are the coordinates spatially dependent but also spin dependent. The electronic density is calculated by integrating the squared absolute value of the wave function over all but one spatial coordinate and summing over the spins σ:

$$\rho(\boldsymbol{r}_1, t) = N \sum_{\sigma(\mathbf{r_1}, \mathbf{r_2}, \ldots, \mathbf{r_N})} \int \cdots \int \psi(\boldsymbol{r}_1, \boldsymbol{r}_2, \ldots, \boldsymbol{r}_N) \psi^*(\boldsymbol{r}_1, \boldsymbol{r}_2, \ldots, \boldsymbol{r}_N)\, d\boldsymbol{r}_2 \cdots d\boldsymbol{r}_N.$$

The time-dependent potential has the form

$$\widehat{V}(t) = \frac{e^2}{4\pi\epsilon_0} \sum_{j=1}^{N} v(\boldsymbol{r}_j, t). \tag{2.2}$$

The term v in (2.2) can be written as

$$v(\boldsymbol{r}, t) = v_0(\boldsymbol{r}) + v_{\text{Ext}}(\boldsymbol{r}, t)\theta(t - t_0),$$

where $v_0(\boldsymbol{r})$ is the local pseudopotential. The potential $v_{\text{Ext}}(\boldsymbol{r}, t)$ is the external potential and θ is the step function given by

$$\theta(t - t_0) = \begin{cases} 1, & t > t_0, \\ 0, & t \leq t_0, \end{cases}$$

i.e., the time-dependent external potential switches on after t_0. Equation (2.1) requires an initial condition. We will assume that the system is in its ground state at $t = t_0$, which will be computed using stationary Kohn–Sham equations.

2.2. TDKS equation with spin polarization. It is numerically difficult and often impossible to obtain a solution to (2.1) for the many-body wave function, as it depends on the coordinates of all the electrons in the system. For this reason, TDDFT has been developed such that instead of solving the wave function in (2.1), the time-dependent electron density, $\rho(\boldsymbol{r}, t)$, is the fundamental variable. To obtain $\rho(\boldsymbol{r}, t)$, TDDFT solves the TDKS equations (1.1). As explained before, the solutions of the TDKS equations $\{\phi_j(\boldsymbol{r}, t)\}_{j=1}^{N}$ are complex valued orbitals with N being the number of electrons in the system. The time-dependent density $\rho(\boldsymbol{r}, t)$ can be obtained through (1.2). For the Kohn–Sham potential (1.3), the nuclear potential $v_0(\boldsymbol{r})$ can be approximated by pseudopotentials, the Hartree potential is given by (1.4) or, equivalently, (1.5), and the exchange-correlation functional will be chosen to be the ALDA approximation in this paper as stated in (1.6).

The TDKS equations with spin dependence, in atomic units, can be given by

$$\mathrm{i}\hbar\partial_t \phi_{j,\sigma} = \left[-\frac{\hbar^2}{2m}\nabla^2 + \frac{e^2}{4\pi\epsilon_0} \left(v_\sigma(\boldsymbol{r}, t) + \int_{\mathbb{R}^3} \frac{n(\boldsymbol{r}', t)}{|\boldsymbol{r} - \boldsymbol{r}'|} + v_{xc}[n_\uparrow, n_\downarrow](\boldsymbol{r}, t) \right) \right] \phi_{j,\sigma}(\boldsymbol{r}, t),$$

where the total density is given by the sum of the spin-up and spin-down densities:

$$n(\boldsymbol{r},t)=\sum_{\sigma=\uparrow,\downarrow} n_\sigma(\boldsymbol{r},t)=\sum_{\sigma=\uparrow,\downarrow}\sum_{j=1}^{N_\sigma}|\phi_{j,\sigma}(\boldsymbol{r},t)|^2.$$

For convenience, we take the spin quantization axis to be the z-axis. This form of the TDKS more closely reflects reality, as electrons have magnetic moments. In this form, the external potential could depend on a time-dependent magnetic field. For numerical experiments, we will rescale the system by using nondimensionalization, which will be done in the following section.

2.3. Nondimensionalizing Schrödinger and Kohn–Sham equations. Now we want to derive the nondimensional time-dependent Schrödinger equation (1.7) from its physical form (2.1) which, for simplicity, can be rewritten as

$$\mathrm{i}\hbar\partial_t\phi=-\frac{\hbar^2}{2m}\nabla^2\phi+V(\boldsymbol{r})\phi. \tag{2.3}$$

Let

$$\widetilde{\boldsymbol{r}}=\boldsymbol{r}/\lambda,\qquad \widetilde{t}=t/\omega,\qquad \text{and}\qquad \widetilde{\phi}_i(\widetilde{\boldsymbol{r}},\widetilde{t})=\lambda^{3/2}\phi_i(\boldsymbol{r},t). \tag{2.4}$$

Upon substitution and multiplying both sides of (2.3) by $\frac{\omega^2}{m\lambda^{1/2}}$, we obtain

$$\mathrm{i}\varepsilon\partial_{\widetilde{t}}\widetilde{\phi}^\varepsilon=-\frac{\varepsilon^2}{2}\nabla^2\widetilde{\phi}^\varepsilon+\frac{\omega^2}{\lambda^2}V(\widetilde{\boldsymbol{r}})\widetilde{\phi}^\varepsilon, \tag{2.5}$$

where ε is now a dimensionless parameter given by

$$\varepsilon:=\frac{\hbar\omega}{m\lambda^2}. \tag{2.6}$$

We write $\widetilde{\phi}^\varepsilon$ to emphasize the dependence of the solution on ε or, equivalently on the parameters λ and ω via (2.6).

The nondimensionalized form for the Kohn–Sham equations can be obtained by replacing the potential from (2.5) with the Kohn–Sham potential v_s, which yields

$$\mathrm{i}\varepsilon\partial_{\widetilde{t}}\widetilde{\phi}_i=-\frac{\varepsilon^2}{2}\widetilde{\nabla}^2\widetilde{\phi}_i+\frac{e^2\omega^2}{4\pi\epsilon_0 m_e\lambda^2}\widetilde{v}_s[\widetilde{\rho}](\widetilde{\boldsymbol{r}},\widetilde{t})\widetilde{\phi}_i, \tag{2.7}$$

where each term of $\widetilde{v}_s[\widetilde{\rho}](\widetilde{\boldsymbol{r}},\widetilde{t})$ is in the same form as the corresponding term in $v_s[\rho](\boldsymbol{r},t)$ but with the rescaling of (2.4). The density is now given by

$$\widetilde{\rho}(\widetilde{\boldsymbol{r}},\widetilde{t})=\sum_{i}^{N} f_i|\widetilde{\phi}_i(\widetilde{r},\widetilde{t})|^2. \tag{2.8}$$

Choosing values for $\omega=au_{\text{time}}\approx 2.41884326\cdot 10^{-17}$ s and $\lambda=au_{\text{length}}=a_0\approx 5.29177210\cdot 10^{-11}$ m with Planck's constant $\hbar$, and the mass of the electron m in MKS units, we obtain $\varepsilon=1$, which is the commonly used atomic units.

Remark 1. For simplicity of presentation, in the rest of the paper, we will adopt the normalized forms of the equations without using the tilde notation.

3. Frozen Gaussian approximation. In this section we discuss the FGA for solving the linear Schrödinger equation

$$\mathrm{i}\varepsilon\partial_t\phi^\varepsilon = -\frac{\varepsilon^2}{2}\nabla^2\phi^\varepsilon + V(\boldsymbol{r})\phi^\varepsilon, \tag{3.1}$$

where $0 < \varepsilon \ll 1$, $V(\boldsymbol{r})$ is smooth, and initial condition $\phi_0^\varepsilon(\boldsymbol{r})$ is in $L^2(\mathbb{R}^3)$. In general, the first order FGA ansatz will be close to the exact solution in the sense

$$\|\phi^\varepsilon_{exact}(\boldsymbol{r},t) - \phi^\varepsilon_{FGA}(\boldsymbol{r},t)\|_{L^2} \le C(t)\varepsilon,$$

where $C(t)$ is a time-dependent constant. Rigorous analysis of this result can be found in [25]. For certain special potentials such as linear potentials, the first order FGA ansatz will yield the exact solution.

3.1. FGA ansatz. We present the first order FGA ansatz for solving equation (3.1) asymptotically as $\varepsilon \to 0$. Denote the Gaussian functions in phase space by

$$G^\varepsilon_{\boldsymbol{q},\boldsymbol{p}}(\boldsymbol{r}) = \exp\left(-\frac{1}{2\varepsilon}|\boldsymbol{r}-\boldsymbol{q}|^2 + \frac{\mathrm{i}}{\varepsilon}\boldsymbol{p}\cdot(\boldsymbol{r}-\boldsymbol{q})\right). \tag{3.2}$$

The first order FGA ansatz is given by

$$\phi^\varepsilon_{FGA}(\boldsymbol{r},t) = \frac{1}{(2\pi\varepsilon)^{9/2}}\int_{\mathbb{R}^9} a(t,\boldsymbol{q},\boldsymbol{p})G^\varepsilon_{\boldsymbol{Q},\boldsymbol{P}}(\boldsymbol{r})e^{\mathrm{i}S(t,\boldsymbol{q},\boldsymbol{p})/\varepsilon}\bar{G}_{\boldsymbol{q},\boldsymbol{p}}(\boldsymbol{r}')\phi_0(\boldsymbol{r}')\,d\boldsymbol{r}'\,d\boldsymbol{p}\,d\boldsymbol{q}, \tag{3.3}$$

where the Gaussian functions in phase space are propagated using the Hamiltonian flow:

$$\frac{d\boldsymbol{Q}}{dt} = \boldsymbol{P}, \tag{3.4}$$

$$\frac{d\boldsymbol{P}}{dt} = -\nabla_{\boldsymbol{Q}}V(\boldsymbol{Q}), \tag{3.5}$$

and the equations for the phase S and amplitude a are given by

$$\frac{dS}{dt} = \frac{1}{2}|\boldsymbol{P}|^2 - V(\boldsymbol{Q}), \tag{3.6}$$

$$\frac{da}{dt} = \frac{a}{2}\mathrm{tr}\left((\partial_{\boldsymbol{z}}\boldsymbol{P} - \mathrm{i}\partial_z\boldsymbol{Q}\nabla^2_{\boldsymbol{Q}}V)Z^{-1}\right) \tag{3.7}$$

with $Z := \partial_{\boldsymbol{z}}(\boldsymbol{Q} + \mathrm{i}\boldsymbol{P})$ and $\partial_{\boldsymbol{z}} := \partial_{\boldsymbol{q}} - \mathrm{i}\partial_{\boldsymbol{p}}$.

Typically, the system of ODEs (3.4)–(3.7) is numerically solved using a symplectic Runge–Kutta method. The coefficients for the Butcher tableau for several orders of accuracy can be found in [24]. In the limit as $\varepsilon \to 0$ (the semiclassical regime), the summation in (3.3) becomes highly local and thus computing a solution using the FGA ansatz (3.3) becomes highly efficient. The algorithm we develop will be applicable for values of ε near 1, as well as for ε in the semiclassical regime. The initial conditions for (3.4)–(3.7) are $\boldsymbol{Q}(0,\boldsymbol{q},\boldsymbol{p}) = \boldsymbol{q}$, $\boldsymbol{P}(0,\boldsymbol{q},\boldsymbol{p}) = \boldsymbol{p}$, $S(0,\boldsymbol{q},\boldsymbol{p}) = 0$, $a(0,\boldsymbol{q},\boldsymbol{p}) = 2^{3/2}$.

3.2. FGA ansatz for lasers. In this section, we will simplify the FGA ansatz for the case of laser potentials $V(\boldsymbol{r})$ of the form:

$$V(\boldsymbol{r}) = \boldsymbol{\alpha} \cdot \boldsymbol{r}$$

or

$$V(\boldsymbol{r}, t) = \boldsymbol{\alpha} \cdot \boldsymbol{r} f(t),$$

where $\boldsymbol{\alpha}$ is a polarization vector and $f(t)$ is a time-dependent profile. We will further derive a fast algorithm for solving the TDKS with laser potentials. Our simplification will involve solving (3.4)–(3.7) exactly and evaluating the integration with respect to $\boldsymbol{q}$ and $\boldsymbol{p}$. These are based on the following lemma.

LEMMA 3.1. *If $V(\boldsymbol{r}, t) := 0$ and $\phi_0(\boldsymbol{r}) \in L^2$, the FGA ansatz* (3.3) *can be simplified to*

$$\phi^{\varepsilon}_{FGA}(\boldsymbol{r}, t) = \frac{1}{(2\pi \mathrm{i}\varepsilon t)^{3/2}} \int_{\mathbb{R}^3} \exp\left(\frac{\mathrm{i}}{2\varepsilon t}|\boldsymbol{r} - \boldsymbol{r}'|^2\right) \phi_0(\boldsymbol{r}')\, d\boldsymbol{r}'. \tag{3.8}$$

Proof. For $V := 0$, the system of ODEs (3.4)–(3.7) can be solved analytically:

$$\begin{aligned} \boldsymbol{Q}(\boldsymbol{q}, \boldsymbol{p}, t) &= \boldsymbol{p}t + \boldsymbol{q}, \\ \boldsymbol{P}(\boldsymbol{q}, \boldsymbol{p}, t) &= \boldsymbol{p}, \\ S(\boldsymbol{q}, \boldsymbol{p}, t) &= \frac{1}{2}|\boldsymbol{p}|^2 t, \\ a(\boldsymbol{q}, \boldsymbol{p}, t) &= \mathrm{i}^{-3/2}(t + 2\mathrm{i})^{3/2}. \end{aligned}$$

Substituting $(\boldsymbol{Q}, \boldsymbol{P}, S, a)$ into (3.3) yields an integrand of the form of an exponential of quadratic functions in $\boldsymbol{q}$ and $\boldsymbol{p}$:

$$\begin{aligned} \phi^{\varepsilon}_{FGA}(\boldsymbol{r}, t) = \frac{1}{(2\pi\varepsilon)^{9/2}} \int_{\mathbb{R}^9} a(t, \boldsymbol{q}, \boldsymbol{p}) \exp\left(-\frac{1}{2\varepsilon}|\boldsymbol{r} - (\boldsymbol{p}t + \boldsymbol{q})|^2 + \mathrm{i}\frac{\boldsymbol{p}}{\varepsilon} \cdot (\boldsymbol{r} - (\boldsymbol{p}t + \boldsymbol{q}))\right) \\ \times \exp\left(\mathrm{i}\frac{|\boldsymbol{p}|^2}{2\varepsilon} t\right) \\ \times \exp\left(-\frac{1}{2\varepsilon}|\boldsymbol{r}' - \boldsymbol{q}|^2 - \mathrm{i}\frac{\boldsymbol{p}}{\varepsilon} \cdot (\boldsymbol{r}' - \boldsymbol{q})\right) \phi_0(\boldsymbol{r}')\, d\boldsymbol{r}'\, d\boldsymbol{q}\, d\boldsymbol{p}. \end{aligned} \tag{3.9}$$

Integrating with respect to $\boldsymbol{q}$ and then $\boldsymbol{p}$ yields the result. ∎

Next we want to present the FGA solution for the particular case where the potential has the form

$$v_{laser}(\boldsymbol{r}) = \boldsymbol{\alpha} \cdot \boldsymbol{r}.$$

THEOREM 3.2. *If $V(\boldsymbol{r}) = \boldsymbol{\alpha} \cdot \boldsymbol{r}$, where $\boldsymbol{\alpha} \in \mathbb{R}^3$ and $\phi_0(\boldsymbol{r}) \in L^2$, the FGA ansatz* (3.3) *can be simplified to*

$$\begin{aligned} &\phi^{\varepsilon}_{FGA}(\boldsymbol{r}, t) \\ &= \frac{1}{(2\pi \mathrm{i}\varepsilon t)^{3/2}} \exp\left(-\frac{\mathrm{i}}{\varepsilon}\boldsymbol{\alpha} \cdot \boldsymbol{r}t - \frac{\mathrm{i}}{6\varepsilon}|\boldsymbol{\alpha}|^2 t^3\right) \int_{\mathbb{R}^3} \exp\left(\frac{\mathrm{i}}{2\varepsilon t}|\boldsymbol{r} - \boldsymbol{r}' - \frac{t^2}{2}\boldsymbol{\alpha}|^2\right) \phi_0(\boldsymbol{r}')\, d\boldsymbol{r}'. \end{aligned} \tag{3.10}$$

Proof. The system of ODEs (3.4)–(3.7) can be solved analytically. The solution is given by

$$\begin{aligned}
\boldsymbol{Q}(\boldsymbol{q},\boldsymbol{p},t) &= -\boldsymbol{\alpha}t^2/2 + \boldsymbol{p}t + \boldsymbol{q},\\
\boldsymbol{P}(\boldsymbol{q},\boldsymbol{p},t) &= -\boldsymbol{\alpha}t + \boldsymbol{p},\\
S(\boldsymbol{q},\boldsymbol{p},t) &= \frac{1}{3}|\boldsymbol{\alpha}|^2t^3 - \boldsymbol{\alpha}\cdot\boldsymbol{p}t^2 + \frac{1}{2}|\boldsymbol{p}|^2t - \boldsymbol{\alpha}\cdot\boldsymbol{q}t,\\
a(\boldsymbol{q},\boldsymbol{p},t) &= \mathrm{i}^{-3/2}(t+2\mathrm{i})^{3/2}.
\end{aligned}$$

Upon substituting the ODE solution $(\boldsymbol{q},\boldsymbol{p},S,a)$ into (3.3), one can analytically compute the integrals with respect to $\boldsymbol{q}$ and $\boldsymbol{p}$. To simplify this calculation, we make the substitution $\boldsymbol{s} = \boldsymbol{r} + \boldsymbol{\alpha}\frac{t^2}{2}$, which will yield

$$\begin{aligned}
\phi^{\varepsilon}_{FGA}(\boldsymbol{s},t) = \frac{N}{(2\pi\varepsilon)^{9/2}}\int_{\mathbb{R}^9} a(t,\boldsymbol{q},\boldsymbol{p})\exp\left(-\frac{1}{2\varepsilon}|\boldsymbol{s}-(\boldsymbol{p}t+\boldsymbol{q})|^2 + \mathrm{i}\frac{\boldsymbol{p}}{\varepsilon}\cdot(\boldsymbol{s}-(\boldsymbol{p}t+\boldsymbol{q}))\right)\\
\times\exp\left(\mathrm{i}\frac{|\boldsymbol{p}|^2}{2\varepsilon}t\right)\exp\left(-\frac{1}{2\varepsilon}|\boldsymbol{r}'-\boldsymbol{q}|^2 - \mathrm{i}\frac{\boldsymbol{p}}{\varepsilon}\cdot(\boldsymbol{r}'-\boldsymbol{q})\right)\phi_0(\boldsymbol{r}')\,d\boldsymbol{r}'\,d\boldsymbol{q}\,d\boldsymbol{p},
\end{aligned}$$

where

$$N = \exp\left(-\frac{\mathrm{i}}{\varepsilon}\boldsymbol{\alpha}\cdot\boldsymbol{s}t - \frac{\mathrm{i}}{3\varepsilon}|\boldsymbol{\alpha}|^2t^3\right).$$

Aside from the factor of N, this integral is precisely of the form of (3.9) for the zero potential. Therefore by Lemma 3.1, this reduces to (3.8) but with $\boldsymbol{r}$ replaced with $\boldsymbol{s}$ and multiplied by N. ∎

Remark 2. In general the FGA yields an error of order $\mathcal{O}(\varepsilon)$ for any given smooth potential; however, (3.10) is the exact solution to the Schrödinger equation with a linear potential.

Now we introduce the integral operator for potentials of the form

$$v_{laser}(\boldsymbol{r},t) = \boldsymbol{\alpha}\cdot\boldsymbol{r}f(t). \tag{3.11}$$

To derive a propagator, we assume that $f(t)$ has a Taylor expansion about $t=0$:

$$f(t) = \sum_{i=0}^{m} a_i t^i. \tag{3.12}$$

We can use similar arguments as in Theorem 3.2 for this potential, and derive the

following system of ODEs:

$$
\begin{aligned}
\boldsymbol{Q}(\boldsymbol{q},\boldsymbol{p},t) &= -\boldsymbol{\alpha}\sum_{i=0}^{m} a_i \frac{t^{i+2}}{(i+1)(i+2)} + \boldsymbol{p}t + \boldsymbol{q},\\
\boldsymbol{P}(\boldsymbol{q},\boldsymbol{p},t) &= -\boldsymbol{\alpha}\sum_{i=0}^{m} a_i \frac{t^{i+1}}{i+1} + \boldsymbol{p},\\
S(\boldsymbol{q},\boldsymbol{p},t) &= \frac{1}{2}|\boldsymbol{\alpha}|^2 \sum_{i=0}^{2m}\left(\sum_{k=0}^{i} \frac{a_k a_{i-k}}{(i+3)(k+1)(i-k+1)}\right) t^{i+3}\\
&\quad - \boldsymbol{\alpha}\cdot\boldsymbol{p}\sum_{i=0}^{m} a_i \frac{t^{i+2}}{(i+1)(i+2)} + \frac{1}{2}|\boldsymbol{p}|^2 t\\
&\quad + |\boldsymbol{\alpha}|^2 \sum_{i=0}^{2m}\left(\sum_{k=0}^{i} \frac{a_k a_{i-k}}{(k+1)(k+2)}\right) \frac{t^{i+3}}{i+3}\\
&\quad - \boldsymbol{\alpha}\cdot\boldsymbol{p}\sum_{i=0}^{m} a_i \frac{t^{i+2}}{i+2} - \boldsymbol{\alpha}\cdot\boldsymbol{q}\sum_{i=0}^{m} a_i \frac{t^{i+1}}{i+1}\\
&= \frac{1}{2}|\boldsymbol{\alpha}|^2 \sum_{i=0}^{2m}\left(\sum_{k=0}^{i} \frac{a_k a_{i-k}(2i-k+4)}{(k+1)(i-k+1)(k+2)}\right) \frac{t^{i+3}}{i+3} - \boldsymbol{\alpha}\cdot\boldsymbol{p}\left(\sum_{i=0}^{m} \frac{a_i}{i+1} t^{i+2}\right)\\
&\quad - \boldsymbol{\alpha}\cdot\boldsymbol{q}\sum_{i=0}^{m} a_i \frac{t^{i+1}}{i+1} + \frac{1}{2}|\boldsymbol{p}|^2 t,\\
a(\boldsymbol{q},\boldsymbol{p},t) &= \mathrm{i}^{-3/2}(t+2\mathrm{i})^{3/2}.
\end{aligned}
$$

When $(\boldsymbol{Q},\boldsymbol{P},S,a)$ are substituted into (3.3), we obtain the simplified ansatz

$$
\begin{aligned}
&\phi^{\varepsilon}_{FGA}(\boldsymbol{r},t)\\
&\quad = \frac{1}{(2\pi\mathrm{i}\varepsilon t)^{3/2}} \exp\left(\frac{\mathrm{i}}{\varepsilon} w - \frac{\mathrm{i}}{\varepsilon}\boldsymbol{T}\cdot(\boldsymbol{r}+\boldsymbol{u})\right) \int_{\mathbb{R}^3} \exp\left(\frac{\mathrm{i}}{2\varepsilon t}|\boldsymbol{r}-\boldsymbol{r}'-\boldsymbol{u}|^2\right) \phi_0(\boldsymbol{r}')\, d\boldsymbol{r}',
\end{aligned}
\tag{3.13}
$$

where

$$
\begin{aligned}
\boldsymbol{u} &:= \boldsymbol{\alpha}\sum_{i=0}^{m} a_i \frac{t^{i+2}}{(i+1)(i+2)},\\
\boldsymbol{T} &:= \boldsymbol{\alpha}\sum_{i=0}^{m} a_i \frac{t^{i+1}}{i+1},\\
w &:= \frac{1}{2}|\boldsymbol{\alpha}|^2 \sum_{i=0}^{2m}\left(\sum_{k=0}^{i} \frac{a_k a_{i-k}(2i-k+4)}{(k+1)(i-k+1)(k+2)}\right) \frac{t^{i+3}}{i+3}.
\end{aligned}
$$

Remark 3. Equation (3.13) is the exact solution to the Schrödinger equation when $f(t)$ is a Taylor expanded function. For a function which is not a finite Taylor series, there will be an error associated with the Taylor expansion.

Remark 4. When the simplified FGA ansatz (3.13) is used to solve the TDKS on a time interval $[t, t+\Delta t]$, one can reduce the number of terms in the Taylor expansion of $f(t)$, by expanding it at the midpoint $t + \Delta t/2$.

3.3. Implementation of the FGA ansatz for lasers. We now describe how to implement (3.10) and (3.13) using the fast (FFT) and inverse FFT (IFFT). We define the Fourier transform of $f \in L^2(\mathbb{R}^3)$ to be

$$\mathcal{F}[f](\boldsymbol{k}) := \int_{\mathbb{R}^3} f(\boldsymbol{r}) e^{-2\pi \mathrm{i} \boldsymbol{r}\cdot\boldsymbol{k}}\, d\boldsymbol{r}.$$

Case 1*:* $V = \boldsymbol{\alpha}\cdot\boldsymbol{r}$. The simplified FGA ansatz (3.10) can be evaluated quickly using the FFT. Notice that

$$\begin{aligned} F(\boldsymbol{k}) &:= \mathcal{F}\left[\exp\left(\frac{\mathrm{i}}{2\varepsilon t}|\boldsymbol{r} - \boldsymbol{\alpha}\frac{t^2}{2}|^2\right)\right] \\ &= (2\pi\varepsilon \mathrm{i}t)^{3/2} \exp(-\pi \mathrm{i} t^2 \boldsymbol{\alpha}\cdot\boldsymbol{k}) \exp\left(-2\mathrm{i}\varepsilon t|\pi\boldsymbol{k}|^2\right). \end{aligned} \tag{3.14}$$

We discretize (3.14) on an even number grid size (N_x, N_y, N_z) so that

$$\begin{aligned} F(\boldsymbol{k}) = (2\pi\varepsilon \mathrm{i}t)^{3/2} &\exp\left(-\pi \mathrm{i} t^2 \boldsymbol{\alpha}\cdot\left(\frac{\boldsymbol{k}_x}{L_x}, \frac{\boldsymbol{k}_y}{L_y}, \frac{\boldsymbol{k}_z}{L_z}\right)\right) \\ &* \exp\left[-2\mathrm{i}\varepsilon t\pi^2\left(\frac{\boldsymbol{k}_x^2}{L_x^2} + \frac{\boldsymbol{k}_y^2}{L_y^2} + \frac{\boldsymbol{k}_z^2}{L_z^2}\right)\right], \end{aligned}$$

where L_x, L_y, and L_z specify the size of the analyzing domain and, $\boldsymbol{k}_x$, $\boldsymbol{k}_y$, and $\boldsymbol{k}_z$ are the 3-dimensional grid coordinates based on the lattice:

$$\begin{aligned} \hat{\boldsymbol{x}} &= [0, 1, 2, \ldots, N_x/2, -N_x/2, -N_x/2+1, \ldots, -1]^T, \\ \hat{\boldsymbol{y}} &= [0, 1, 2, \ldots, N_y/2, -N_y/2, -N_y/2+1, \ldots, -1]^T, \\ \hat{\boldsymbol{z}} &= [0, 1, 2, \ldots, N_z/2, -N_z/2, -N_z/2+1, \ldots, -1]^T. \end{aligned}$$

The product $\boldsymbol{k}_j^2 = \boldsymbol{k}_j .* \boldsymbol{k}_j$ is done elementwise. The FGA ansatz for the case of lasers is then evaluated by

$$\phi_{FGA}^{\varepsilon}(\boldsymbol{r}, t) = \exp\left(-\frac{\mathrm{i}}{\varepsilon}\boldsymbol{\alpha}\cdot\boldsymbol{r}t - \frac{\mathrm{i}}{6\varepsilon}|\boldsymbol{\alpha}|^2 t^3\right) IFFT\left[F(\boldsymbol{k}) .* FFT(\phi_0(\boldsymbol{r}))\right]. \tag{3.15}$$

Remark 5. The ordering of elements in the lattice vectors $\hat{\boldsymbol{x}}$, $\hat{\boldsymbol{y}}$, $\hat{\boldsymbol{z}}$ is for the convenience of not having to shift the spectrum.

Case 2*:* $V = \boldsymbol{\alpha}\cdot\boldsymbol{r}f(t)$. The simplified FGA ansatz (3.13) can be evaluated almost the same way as in Case 1 above. The main difference is that now the Fourier transform has the form

$$\begin{aligned} F(\boldsymbol{k}) &:= \mathcal{F}\left[\exp\left(\frac{\mathrm{i}}{2\varepsilon t}|\boldsymbol{r} - \boldsymbol{u}|^2\right)\right], \\ &= (2\pi\varepsilon \mathrm{i}t)^{3/2} \exp(-2\pi \mathrm{i}\boldsymbol{u}\cdot\boldsymbol{k}) \exp\left(-2\mathrm{i}\varepsilon t|\pi\boldsymbol{k}|^2\right), \end{aligned}$$

which we discretize as

$$F(\boldsymbol{k}) = (2\pi\varepsilon \mathrm{i}t)^{3/2} \exp\left(-2\pi \mathrm{i}\boldsymbol{u}\cdot\left(\frac{\boldsymbol{k}_x}{L_x}, \frac{\boldsymbol{k}_y}{L_y}, \frac{\boldsymbol{k}_z}{L_z}\right)\right) * \exp\left[-2\mathrm{i}\varepsilon t\pi^2\left(\frac{\boldsymbol{k}_x^2}{L_x^2} + \frac{\boldsymbol{k}_y^2}{L_y^2} + \frac{\boldsymbol{k}_z^2}{L_z^2}\right)\right].$$

The FGA ansatz is then given by

$$\phi_{FGA}^{\varepsilon}(\boldsymbol{r}, t) = \exp\left(\frac{\mathrm{i}}{\varepsilon}w - \frac{\mathrm{i}}{\varepsilon}\boldsymbol{T}\cdot(\boldsymbol{r} + \boldsymbol{u})\right) IFFT\left[F(\boldsymbol{k}) .* FFT(\phi_0(\boldsymbol{r}))\right]. \tag{3.16}$$

4. FGA method for the Kohn–Sham equations. In this section we present our algorithm and its implementation for solving the TDKS equations.

4.1. Single-step predictor-corrector algorithm for the TDKS equations. Because of the nonlinearity of the system of (2.7) and (2.8), we will solve it iteratively until self-consistency is reached. To this end, we will use a predictor-corrector algorithm. First, we will assume that the ground state density along with the N ground state Kohn–Sham orbitals $\{\phi_j(\boldsymbol{r}, t_0)\}_{j=1}^N$ have been precomputed using ground states Kohn–Sham equations, which has the following form in atomic units:

$$\left[-\frac{1}{2}\nabla^2 + v_s[\rho](\boldsymbol{r})\right]\phi_j = \epsilon_j\phi_j, \qquad j = 1, 2, \ldots, N, \tag{4.1}$$

where $\rho(\boldsymbol{r})$ is defined the same as in (1.2) and

$$v_s[\rho](\boldsymbol{r}) = v_0(\boldsymbol{r}) + \int \frac{\rho(\boldsymbol{r})}{|\boldsymbol{r} - \boldsymbol{r}'|}d\boldsymbol{r}' + v_{xc}[\rho](\boldsymbol{r}).$$

As mentioned earlier, $v_0(\boldsymbol{r})$ is a pseudopotential, the second term in $v_s[\rho(r)]$ is the Hartree potential, and v_{xc} is the exchange-correlation potential. The Kohn–Sham eigenvalues ϵ_i have corresponding eigenfunctions (orbitals) ϕ_j for $j = 1, 2, \ldots, N$, and are the lowest N eigenvalues of the Kohn–Sham Hamiltonian operator. There are many freely available software for solving (4.1), e.g., *Octopus* [1], which we will be using for computing the ground state density and orbitals in numerical examples in the next section. We will not discuss details on how to solve equations (4.1), as our main goal is to present time-dependent simulations, and the ground state orbitals will serve as initial conditions for the TDKS equations.

We now describe our single-step predictor-corrector method. Suppose $0 = t_0 < t_1 < t_2 < \cdots < t_M = T$ is a partition of the interval $[0, T]$. To obtain the solution (orbitals and density) at time step t_{j+1} from that at time t_j using an (approximately) unitary propagation, we produce a Hamiltonian $\widetilde{H}^{(n)}(t_j + \Delta t/2)$ compatible with $\phi_i(\boldsymbol{r}, t_j)$ and $\phi_i^{(n)}(\boldsymbol{r}, t_{j+1}) \approx e^{-\mathrm{i}\widehat{H}^{(n)}(t_j+\Delta t/2)}\phi_i(\boldsymbol{r}, t_j)$. The superscript n is the number of corrector steps and $\Delta t/2$ is half the length of $[t_j, t_{j+1}]$.

Step 1 *(Predictor):* We make the initial guess for $\phi_i(\boldsymbol{r}, t_{j+1})$ by advancing the orbitals $\phi_i(\boldsymbol{r}, t_j)$ with the Hamiltonian evaluated at t_j.

Step 2 *(Corrector):* Update the Hamiltonian at time $t_j + \Delta t/2$ using the interpolation

$$\widehat{H}^{(n)}(t_j + \Delta t/2) = \frac{1}{2}\left[\widehat{H}(t_j) + \widehat{H}^{(n)}(t_{j+1})\right]. \tag{4.2}$$

$\widehat{H}^{(n)}(t_{j+1})$ is the Hamiltonian corresponding to $\phi^{(n)}(\boldsymbol{r}, t_{j+1})$. Use the refined Hamiltonian $\widehat{H}^{(n)}(t_j + \Delta t/2)$ to obtain a refined guess for $\phi_i^{(n)}(\boldsymbol{r}, t_{j+1})$. Here $n = 1$ if only Steps 1 and 2 are performed.

Step 3*:* For $n > 1$, repeat Step 2 until self-consistency is established.

Implementation of Steps 1 *and* 2*:* We give additional details here on how to advance the orbitals using the spectral algorithm for linear equations driven by lasers which we derived in the previous section. To incorporate the pseudo, Hartree, and exchange-correlation potentials in v_s, we use the following time-splitting scheme such that the equation

$$\mathrm{i}\varepsilon\partial_t\phi = -\frac{\varepsilon^2\nabla^2}{2}\phi + (v_{laser} + v_0 + v_h + v_{xc})\phi$$

will be split into three steps and solved on the interval $[t_j, t_{j+1}]$:

$$\mathrm{i}\varepsilon\partial_t\phi^* = \frac{(v_0 + v_h + v_{xc})}{2}\phi^*, \quad \phi_0^*(\boldsymbol{r}) = \phi(\boldsymbol{r}, t_j), \tag{4.3}$$

$$\mathrm{i}\varepsilon\partial_t\phi^{**} = (-\frac{\varepsilon^2\nabla^2}{2} + v_{laser})\phi^{**}, \quad \phi_0^{**}(t_j) = \phi^*(t_{j+1}), \tag{4.4}$$

$$\mathrm{i}\varepsilon\partial_t\phi = \frac{(v_0 + v_h + v_{xc})}{2}\phi, \quad \phi_0(t_j) = \phi^{**}(t_{j+1}), \tag{4.5}$$

i.e., the initial conditions: $\phi_0(\boldsymbol{r}) = \phi(\boldsymbol{r}, t_j)$ is chosen for (4.3), then the solution to (4.3) at time t_{j+1} will be used as the initial condition for (4.4); finally for (4.5), the initial condition will be the solution to (4.4) at time t_{j+1}.

The exact solution to (4.3) and (4.5) is given by

$$\tilde{\phi}(\boldsymbol{r}, t_{j+1}) = \exp\left(\int_{t_j}^{t_{j+1}} \frac{-\mathrm{i}(v_0(\boldsymbol{r}) + v_h(\boldsymbol{r}, s) + v_{xc}(\boldsymbol{r}, s))}{2\varepsilon} ds\right) \tilde{\phi}_0(\boldsymbol{r}, t_j).$$

However, we will approximate the solution to the above splitting (4.3)–(4.5) by

$$\begin{aligned} \phi^* &= \exp\left(-\frac{\mathrm{i}}{2\varepsilon}\Delta t(v_0(\boldsymbol{r}) + v_h(\boldsymbol{r}, t^*) + v_{xc}(\boldsymbol{r}, t^*))\right)\phi_0(\boldsymbol{r}, t_j), \\ \phi^{**} &= \phi_{laser} \text{ using (3.15) or (3.16) with initial condition } \phi^*, \\ \phi(\boldsymbol{r}, t_{j+1}) &= \exp\left(-\frac{\mathrm{i}}{2\varepsilon}\Delta t(v_0(\boldsymbol{r}) + v_h(\boldsymbol{r}, t^*) + v_{xc}(\boldsymbol{r}, t^*))\right)\phi^{**}, \end{aligned} \tag{4.6}$$

where $t^* \in [t_j, t_{j+1}]$. Now that we have evolved each of the orbitals ϕ_i to time t_{j+1}, the density $\rho(\boldsymbol{r}, t_{j+1})$ can be obtained. This should not be the final solution for the time-dependent density, as we do not know a priori $v_s(\boldsymbol{r}, t)$ for $t \in [t_j, t_{j+1}]$, but it is a good first guess. To obtain a more accurate approximate density we repeat Step 2 iteratively, which is actually done in the corrector part of our algorithm.

Remark 6. Comparing this with the Strang-splitting spectral method in [5], where the splitting is done as

$$\begin{aligned} \phi^* &= \exp\left(-\frac{\mathrm{i}\Delta t}{2\varepsilon}\widehat{V}\right)\phi_0(\boldsymbol{r}, t_j), \\ \phi^{**} &= \exp\left(-\frac{\mathrm{i}\Delta t}{\varepsilon}\widehat{D}\right)\phi^*, \\ \phi(\boldsymbol{r}, t_{j+1}) &= \exp\left(-\frac{\mathrm{i}\Delta t}{2\varepsilon}\widehat{V}\right)\phi^{**}, \end{aligned} \tag{4.7}$$

where $\widehat{D} := -\frac{\varepsilon^2\nabla^2}{2}$ and $\widehat{V} := v_s(\boldsymbol{r}, t)$, one can see that our algorithm deals with the external potential more efficiently.

The single-step predictor-corrector algorithm outlined above is a midpoint approximation. This approximation has the advantage of preserving the unitary in time evolution of the Schrödinger equation. The phrase *single-step method* is used for algorithms which obtain the solution one time step at a time. Compared with the *global* methods that usually consists of making a guess for $\rho(\boldsymbol{r}, t_j)$ for all the $\{t_j\}_{j=1}^N$ before applying the corrector step, numerically, the single-step method is more stable due to the preservation of the unitary.

4.2. Implementation of absorbing boundary conditions for ionization. To deal with possible ionization, (4.6) is usually multiplied by a smooth cutoff function $\mathcal{C}(\boldsymbol{r})$, which is equal to 1 in the analyzing region $\mathcal{M}$ and smoothly decays to 0 at some specified distance away from $\mathcal{M}$. Alternatively, if one is computing the solution of the linear Schrödinger equation using the FGA ansatz (3.3), there is no need to construct a smooth cutoff function for the FGA method if we compute the summation of the phase-space Gaussian function (3.2) in the following way: when the center of the (3.2) $\boldsymbol{Q}^i(\boldsymbol{q}_0^i, \boldsymbol{p}_0^i, t)$ is located at a distance greater than $\mathcal{O}(\sqrt{\varepsilon})$ from $\mathcal{M}$, omit the index i in the summation of (3.2). We choose a distance $\mathcal{O}(\sqrt{\varepsilon})$ from $\mathcal{M}$ because the Gaussian functions have standard deviation $\sqrt{\varepsilon}$. The solution will smoothly decay to zero outside $\mathcal{M}$ as it was constructed as a superposition of Gaussian functions, therefore, we do not have to multiply the solution with a smooth cutoff function after each time step. This kind of absorbing boundary conditions was also constructed in [8].

5. Numerical examples. In this section we will present numerical examples to test our spectral algorithm. We will simply refer it as the FGA-based algorithm as it was derived using the FGA ansatz. We will compare our algorithm with the Crank–Nicolson method and the Strang-splitting spectral method (SSSM). The ALDA approximation for the exchange-correlation potential will be adopted.

Example 5.1. In this example we apply our FGA-based algorithm to a system of 57 valence 1 electron atoms separated at a distance of 4 a.u. (atomic units) and arranged in a stable face centered cubic configuration. Initially the system will be in its ground state as computed using Kohn–Sham DFT. The spatial mesh size used is $\Delta x = \Delta y = \Delta z = 0.5$ a.u. We propagate the system up to time $T = 1.25$ using the external potential

$$v_{ext}(\boldsymbol{r}, t) = x.$$

The pseudopotential is of the form

$$v_0(\boldsymbol{r}) = \sum_{i=1}^{57} \frac{-1}{\sqrt{1 + |\boldsymbol{r} - \boldsymbol{R}_i|^2}},$$

where $\boldsymbol{R}_i$ gives the location of each atom. We display the densities using the FGA-based algorithm and the Crank–Nicolson scheme in Figure 1. As can be seen by Figure 2, the densities differ the most near the location of the nuclei. This difference is due to the smoothness of our spectral method.

Example 5.2. We now consider the same system as in Example 5.1. This time we test the propagator given in (3.13). We propagate the system up to time $T = 4.0$ using the external potential

$$v_{Ext}(\boldsymbol{r}, t) = 2x \cos(\pi t).$$

We will use a fourth order Taylor expansion for (3.12), and compare the dipole moment along the x direction,

$$d_x(t) = \int_{\mathbb{R}^3} x\rho(\boldsymbol{r}, t)\, d\boldsymbol{r},$$

using the FGA-based algorithm and the Crank–Nicolson scheme. Figure 3 displays the dipole moments computed using the FGA-based algorithm and the Crank–Nicolson

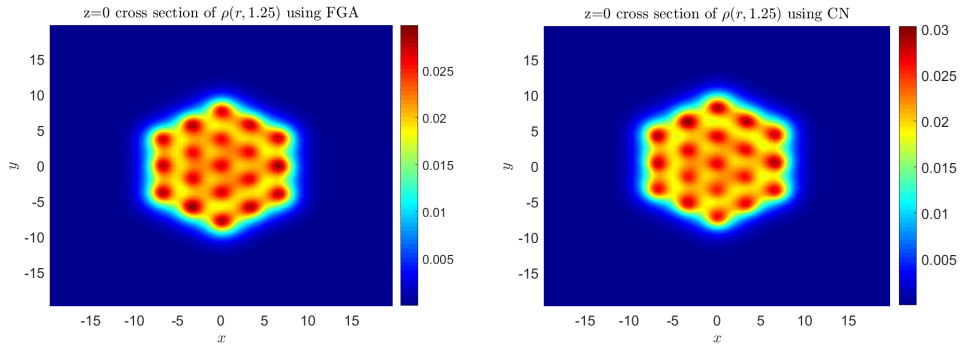

FIG. 1. *Plot of the $z = 0$ cross section of the densities.*

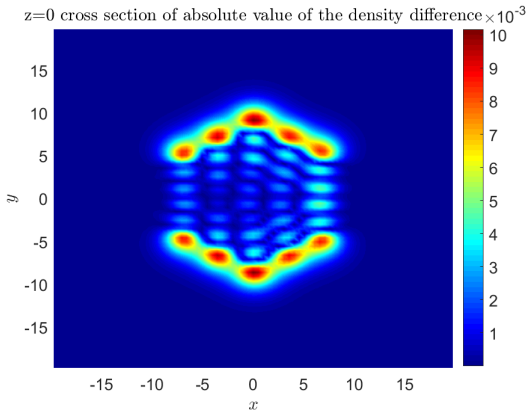

FIG. 2. *Plot of the $z = 0$ cross section of the difference in densities using the FGA-based algorithm and the Crank–Nicolson algorithm.*

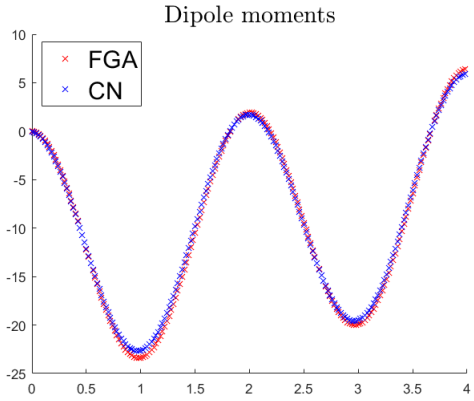

FIG. 3. *Plot of the dipole moments computed obtained using the FGA-based algorithm and the Crank–Nicolson (CN) scheme for Example* 5.2.

scheme. Figure 4 shows the absolute value of the difference between these two algorithms. The runtime for our FGA-based method is 34.9 minutes whereas the Crank–Nicolson scheme takes 82.0 minutes. The error tolerance for the predictor-corrector

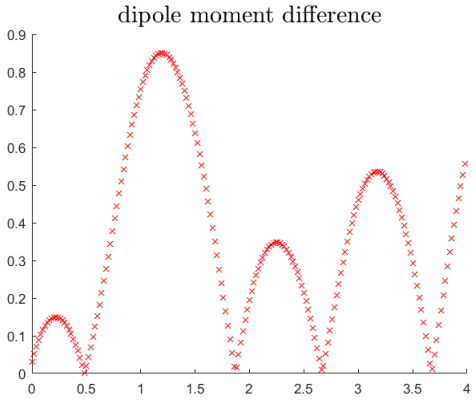

FIG. 4. *Absolute value of the difference in the dipole moments for Example* 5.2.

part was chosen to be 10^{-7}. We implemented our algorithm using MATLAB on a single processor machine, using no parallelization such as multicore processing or GPUs. The Crank–Nicolson scheme was conducted using Octopus [1]. Compared with the previous example, the FFT significantly speeds up the computation. Had we used more advanced computing architectures to implement our algorithm, we would probably see an even faster runtime.

Example 5.3. In this example we will again use the system in Example 5.1. A common choice of external potential used in physics simulations is the Gaussian pulse external field,

$$v_{Ext}(\boldsymbol{r},t) = Ax\exp\left(-(t-827/2)^2/(2\sigma)\right)\cos\left(\omega(t-827/2)\right). \tag{5.1}$$

We choose parameters $A = 0.005$ (or $8.773\cdot 10^{11}$ W/cm^2), $\omega = 2.0/27.211$ (or 2.0 eV), and $\sigma = 1/0.00004$ with final propagation time of 827 a.u. (or about 20 femtoseconds). Our goal is to test two things: the performance of our algorithm over a long time propagation and performance with respect to the size of the domain. We compute the solution of the TDKS equations using an FGA-based spectral method using two different sized domains: $[-12,12]^3$ and $[-16,16]^3$. Our reference solution is computed using the Crank–Nicolson scheme with a large spatial domain and small time steps. To test the performance of the FGA-based algorithm we plot the dipole moments in Figure 5. As is seen on the right side of Figure 5, using a larger domain produces better results. Generally the domain size for our type of spectral method needs to be large enough so that a significant part of the orbitals do not leave the domain.

Example 5.4. In this example we consider a simplified model where the pseudopotential for the system is of the form

$$v_0(\boldsymbol{r}) = -\exp\left(-|\boldsymbol{r}/8|^2\right).$$

The external potential is given by

$$v_{ext}(\boldsymbol{r},t) = 8x\cos(4t).$$

We compute the dipole moments along the x direction from $t = 0$ to $t = 1$ using three

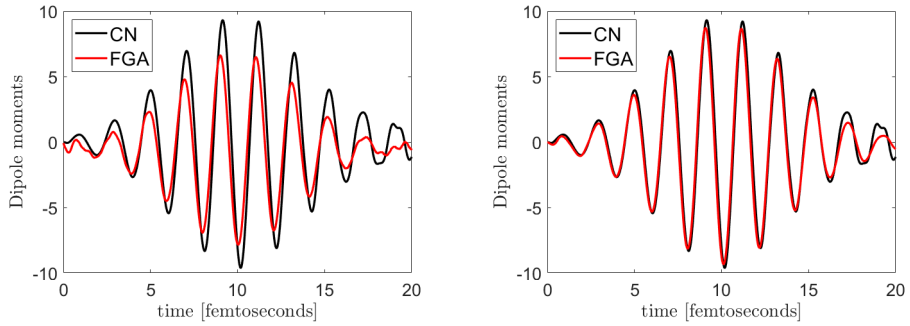

FIG. 5. *Dipole moments. Left: domain size* $[-12, 12]^3$. *Right: domain size* $[-16, 16]^3$.

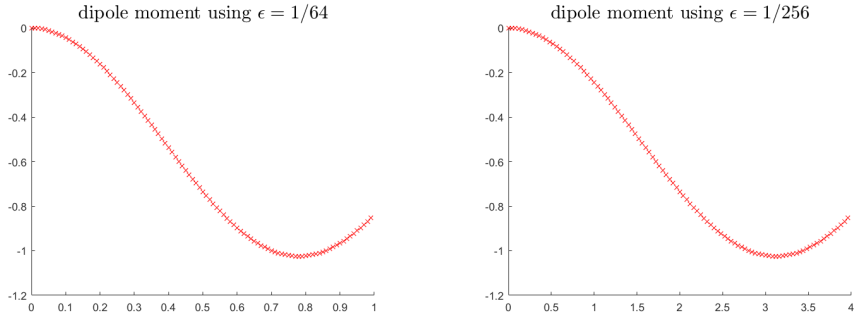

FIG. 6. *Dipole moments for Example* 5.4 *computed using different scalings.*

different scalings:

$$\text{case 1: } \widetilde{\boldsymbol{r}} = \boldsymbol{r} \text{ and } \widetilde{t} = t;$$
$$\text{case 2: } \widetilde{\boldsymbol{r}} = \boldsymbol{r}/8 \text{ and } \widetilde{t} = t;$$
$$\text{case 3: } \widetilde{\boldsymbol{r}} = \boldsymbol{r}/8 \text{ and } \widetilde{t} = t/(1/4).$$

According to (2.6), cases 1, 2, and 3 correspond to $\varepsilon = 1, 1/64$, and $1/256$, respectively. We display our dipole calculation for the last two cases in Figure 6. We note that the figure for $\varepsilon = 1/256$ ranges from 0 to 4 due to the different time scales. The plots of the dipole moments should be highly identical, as our algorithm computes the solution of the linearized equations exactly. As can be seen from these results, our algorithm could also provide a potential use for systems modeled in the semiclassical regime where $0 < \varepsilon \ll 1$. We note that the parameter ε is a degree of measure between quantum and classical mechanics for which when $\varepsilon \to 0$ the classical limit is attained. In general, a small value of ε typically means that one has to smooth the potential v_s in order to simulate the system using the scales of ε. We also note that the FGA solution (3.3) is exact for linear and quadratic potentials. Thus, there is no asymptotic error in this example. For other potentials, the asymptotic error decreases as $\varepsilon \to 0$.

For our last example we verify the claim that our algorithm generally computes the solution of the TDKS more accurately when compared to methods that discretize the external potential. The high accuracy of our algorithm is due to its ability to incorporate the dynamics of the external potential for each time t.

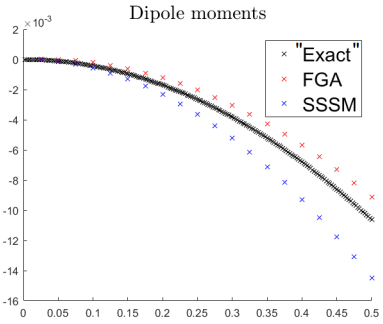

FIG. 7. *Dipole moments for Example* 5.5.

Example 5.5. We consider the same system as in Example 5.4. We use the external potential given by

$$v_{ext}(\boldsymbol{r}, t) = x(20t - 800t^2) \quad \text{for } t = mod(t, 0.025).$$

We compute the dipole moments with respect to x up to time $t = 1/2$ in two ways: using our algorithm (FGA), and using a TDKS solver based on the SSSM which uses a midpoint approximation for the external potential. For demonstration, we omit the corrector part for both algorithms and use the same time step. The exact solution is computed using a time step much smaller than those used for the FGA and SSSM algorithms. As seen in Figure 7, the FGA algorithm is more closer to the "exact" solution as it more efficiently treats the external potential.

6. Conclusion and future work. Our work derives a spectral algorithm for solving the TDKS equations. We use a predictor-corrector algorithm to determine the time evolution of the TDKS. Because our algorithm uses an FFT (and an IFFT), it is faster than algorithms based on finite element methods and has spectral accuracy. Our approach to solving the linear Schrödinger equation is to make the splitting (4.3)–(4.5) and making use of the Fourier integral operator known as the FGA. The main advantage is that we will obtain a smooth solution which will be stable when compared with the WKB or standard GB methods. Our algorithm is formulated in terms of the semiclassical parameter ε, which allows further applications for systems in the semiclassical regime. Another benefit of this approach is that our algorithm incorporates the external potential $v_{ext}(\boldsymbol{r}, t)$ exactly, and therefore tends to converge faster when compared to other methods which use a numerical approximation. Furture study will be focused on optical responses of metal nano structures (see [2], [3]).

REFERENCES

[1] X. ANDRADE ET AL., *Real-space grids and the octopus code as tools for the development of new simulation approaches for electronic systems*, Phys. Chem. Chem. Phys., 17 (2015), pp. 31371–31396.

[2] G. BAO, D. LIU, AND S. LUO, *A multiscale method for optical responses of nanostructures*, SIAM J. Appl. Math., 73, (2013), pp. 741–756.

[3] G. BAO, D. LIU, AND S. LUO, *Multiscale modeling and computation of optically manipulated nano devices*, J. Comput. Phys., 316 (2016), pp. 558–572.

[4] W. BAO, D. JAKSCH, AND P. MARKOWICH, *Numerical solution of the Gross-Pitaevskii equation for Bose-Einstein condensation*, J. Comput. Phys., 187 (2003), pp. 318–342.

[5] W. Bao, S. Jin, and P. Markowich, *On time-splitting spectral approximations for the Schrödinger equation in the semiclassical regime*, J. Comput. Phys., 175 (2002), pp. 487–524.

[6] A. Bensoussan, J. L. Lions, and G. Papanicolaou, *Asymptotic Analysis for Periodic Structures*, North-Holland, Amsterdam, 1978.

[7] A. Castro, M. A. L. Marques, and A. Rubio, *Propagators for the time-dependent Kohn-Sham equations*, J. Chem. Phys., 121 (2004), pp. 3425–3433.

[8] R. Delgadillo, X. Yang, and J. Zhang, *Frozen Gaussian approximation-based artificial boundary conditions for one-dimensional nonlinear Schrödinger equation in the semiclassical regime*, J. Sci. Comput., 75, (2018), pp. 1701–1720.

[9] E. K. U. Gross and E. Runge, *Density-functional theory for time-dependent systems*, Phys. Rev. Lett., 52 (1983), pp. 997–1000.

[10] M. F. Herman and E. Kluk, *A semiclassical justification for the use of non-spreading wavepackets in dynamics calculations*, Chem. Phys., 91 (1984), pp. 27–34.

[11] S. Jin, H. Wu, and X. Yang, *Gaussian beam methods for the Schrödinger equation in the semiclassical regime: Lagrangian and Eulerian formulations*, Commun. Math. Sci., 6 (2008), pp. 995–1020.

[12] J. Lu and X. Yang, *Frozen Gaussian approximation for high frequency wave propagation*, Commun. Math. Sci., 9 (2011), pp. 663–683.

[13] J. Lu and X. Yang, *Convergence of frozen Gaussian approximation for high frequency wave propagation*, Comm. Pure Appl. Math., 65 (2012), pp. 759–789.

[14] J. Lu and X. Yang, *Frozen Gaussian approximation for general linear strictly hyperbolic systems: Formulation and Eulerian methods*, Multiscale Model. Simul., 10 (2012), pp. 451–472.

[15] B. I. Lundqvist and O. Gunnarsson, *Exchange and correlation in atoms, molecules, and solids by the spin density functional formalism*, Phys. Rev. B (3), 13 (1976), pp. 4274–4298.

[16] P. Markowich, P. Pietra, and C. Pohl, *Numerical approximation of quadratic observable of Schrödinger-type equations in the semiclassical limit*, Numer. Math., 81 (1999), pp. 595–630.

[17] P. A. Markowich, P. Pietra, C. Pohl, and H. P. Stimming, *A Wigner-measure analysis of the Dufort–Frankel scheme for the Schrödinger equation*, SIAM J. Numer. Anal., 40 (2002), pp. 1281–1310.

[18] M. A. L. Marques, *Fundamentals of Time Dependent Density Functional Theory*, Springer, Berlin, 2012.

[19] G. Panati, H. Spohn, and S. Teufel, *Effective dynamics for Bloch electrons: Peierls substitution and beyond*, Comm. Math. Phys., 242 (2003), pp. 547–578.

[20] G. Panati, H. Spohn, and S. Teufel, *Motions of electrons in adiabatically perturbed periodic structures*, in Analysis, Modeling and Simulation of Multiscale Problems, Springer, Berlin, 2006, pp. 595–617.

[21] J. P. Perdew and A. Zunger, *Self-interaction correction to density-functional approximations for many electron systems*, Phys. Rev. B (3), 23, (1981), pp. 5048–5079.

[22] M. Popov, *A new method of computation of wave fields using Gaussian beams*, Wave Motion, 4 (1982), pp. 85–97.

[23] C. Ringhofer, *Computational methods for semiclassical and quantum transport in semiconductor devices*, Acta Numer., 6 (1997), pp. 485–521.

[24] G. Sun, *A simple way constructing symplectic Runge-Kutta methods*, Math. Comp., 18 (2000), pp. 61–68.

[25] T. Swart and V. Rousse, *A mathematical justification for the Herman-Kluk propagator*, Commun. Math. Phys., 286 (2009), pp. 725–750.

[26] C. A. Ullrich, *Time-Dependent Density Functional Theory: Concepts and Applications*, Oxford University Press, New York, 2012.